Quantum state protection from finite-temperature thermal noise with application to controlled quantum teleportation

Chi Wang(王驰)[†], Sajede Harraz[†‡], Jiao-Yang Zhang(张骄阳)[†], and Shuang Cong(丛爽)

Department of Automation, University of Science and Technology of China, Hefei 230027, *China*

(Received 11 November 2022; revised manuscript received 7 February 2023; accepted manuscript online 20 February 2023)

We propose a quantum state protection scheme via quantum feedforward control combined with environment-assisted measurement to protect arbitrary unknown initial states from the finite-temperature thermal noise (FTTN). The main strategy is to transfer the quantum system to a noise-robust state by weak measurement and feedforward control before the noise channel. Then we apply the environment-assisted measurement on the noise channel to select our desired damped states that are invertible to the initial state. After the noise channel, the reversal operations are applied to restore the initial state. We consider the protection of a single-qubit system, derive the analytical expressions of the success probability and the fidelity, and analyze the influence of key parameters on the performance of the proposed scheme. Unlike previous studies, there is no trade-off between the fidelity and the success probability in the proposed scheme; hence one could maximize them separately. Simulation results show that the proposed scheme can greatly improve the fidelity of the quantum state with a certain success probability. Moreover, the proposed scheme is successfully applied to improving the fidelity of controlled quantum teleportation through two independent FTTN channels from the perspective of protecting the shared entanglement.

Keywords: quantum feedforward control, environment-assisted measurement, weak measurement, quantum teleportation

PACS: 03.67.Pp, 03.65.Yz, 03.65.Ud **DOI:** 10.1088/1674-1056/acbd2a

1. Introduction

Generally, all real quantum systems interact with the external environment and suffer from decoherence, which is undoubtedly unfavorable to the concrete realization of quantum information theories.[1–3] For instance, in the standard quantum teleportation protocol, the EPR pair (Bell state) shared by the sender and the receiver is used as the communication channel,[4,5] and the presence of environmental noises reduces the entanglement degree and thus affects the transmission effect. Additionally, the implementation of various quantum algorithms in quantum computers also relies on the coherent superposition of quantum states.[6,7] Hence, it is crucial to investigate decoherence control for real quantum systems. A variety of quantum state protection schemes have been proposed to suppress the effects of noise, including quantum error correction,[8–12], decoherence-free subspaces[13–16] and quantum dynamical decoupling.[17–22] However, quantum error correction requires too many redundant qubits; decoherence-free subspace requires the interaction Hamiltonian to have appropriate symmetry; quantum dynamical decoupling requires the generation of ultra-high frequency control pulses. Hence, how to develop practical quantum state protection schemes still remains an opening issue.

Fortunately, quantum state protection schemes based on weak measurement (WM) have shown promising application prospects.[23–25] These schemes mainly include quantum feedback control (QFBC),[26–31] quantum measurement and its reversal,[32–35] and quantum feedforward control (QFFC).[36,37] In Ref. [26], the QFBC scheme was proposed to protect a class of single-qubit states from the phase damping (PD) noise, where weak measurements are used after the noise channel to gain the information of the system state and the noise, and then rotation operators are employed to correct the damped state. Later, it was verified that QFBC schemes could also protect single-qubit states from the other types of noises, e.g., the amplitude damping (AD) noise, the bit-flip noise and the depolarizing noise.[38,39] However, QFBC schemes rely on the prior information on the initial state and assume the initial state to be completely known. In fact, the prior information on quantum states before the noise channel is essential to the optimum suppression of noises.[34,35] In Ref. [32], the WM and its reversal scheme was proposed to protect arbitrary unknown single-qubit states from the AD noise, which uses WM to obtain partial information on the initial state before the noise channel, and then apply a WM reversal to recover the quantum state after the noise channel.[33–35] Furthermore, in Ref. [36], the QFFC scheme was presented as an upgraded version of the WM and its reversal scheme, which uses feedforward operators after the pre-WMs before the noise channel, and reversed feedforward operators before the post-WMs after the noise channel. In fact, the QFFC scheme follows the same idea as the previous WM and its reversal scheme but outperforms

[†]These authors contributed equally to this work.

[‡]Corresponding author. E-mail: sajede@ustc.edu.cn

© 2023 Chinese Physical Society and IOP Publishing Ltd

it, since the initial state can certainly be transferred to a state that is robust to noise by adding the feedforward operators. In Ref. [37], the QFFC scheme was extended to the protection of arbitrary unknown two-qubit states, and its performance was analyzed in detail. It should be noted that the AD and the PD noises mentioned above only exist at zero-temperature. However, in many practical quantum systems, e.g., superconducting circuits and Rydberg atomic systems, the zero-temperature assumption is not valid and the thermal environment needs to be considered; otherwise, the error caused by noise model would not be tolerable. In these cases, modeling the quantum noise as the finite-temperature thermal noise (FTTN) is more consistent with the real environment.[40]

In this paper, motivated by the previous QFFC schemes,[32–37] we investigate the protection of arbitrary unknown quantum states from FTTN via QFFC combined with environment-assisted measurement (EAM). Theoretically, the designed scheme is suitable for protecting quantum states from arbitrary types of quantum noises with at least one invertible Kraus operator, though the strengths of WMs need redesigning for different types of noises. Analytical expressions of the total fidelity and the corresponding success probability are presented to evaluate the performance of the proposed scheme. Furthermore, the optimal conditions in the sense of maximizing the total fidelity and the total success probability are derived, respectively, where the optimal values of the pre- and the post-WM strengths are given. For comparison, we consider the QFFC scheme in Ref. [41] to highlight the superiority of our proposed scheme. Finally, the proposed scheme is applied to the protection of controlled quantum teleportation through FTTN channels. Simulations are performed to demonstrate that the proposed scheme can improve the fidelity of controlled quantum teleportation from the perspective of protecting the shared entanglement without modifying the quantum teleportation protocol.

The remainder of this paper is organized as follows. In Section 2, we elaborate the protection of a single-qubit system under the influence of FTTN. In Section 3, we apply the protection scheme to the controlled quantum teleportation through FTTN channels. Finally, conclusions are drawn in Section 4.

2. Quantum state protection from FTTN for a single-qubit system

This section is concerned with the protection of a single-qubit system from FTTN via QFFC combined with EAM. Hereafter, we call our proposed scheme as QFFC-EAM. According to the characteristics of the FTTN channel, we first use the pre-WM operators and feedforward operators to transfer the system state to a less vulnerable state before entering the FTTN channel, then apply the EAM to the FTTN channel, and finally apply the reversed feedforward operators and the post-WM operators after the FTTN channel to restore the damped state to its initial state. The schematic diagram of the whole quantum state protection scheme is shown in Fig. 1.

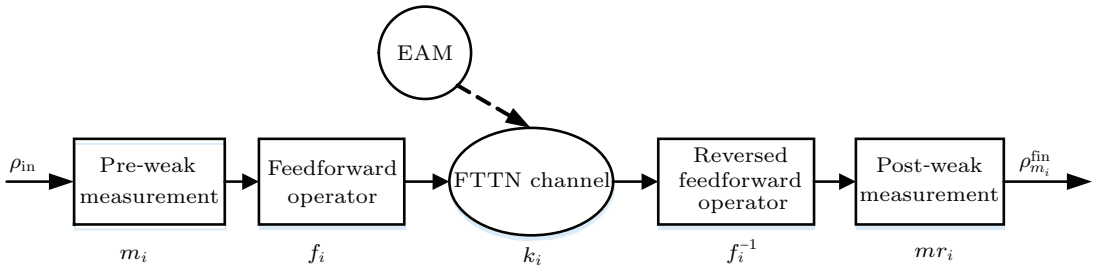


Fig. 1. Schematic diagram of QFFC-EAM.

The whole quantum state protection scheme consists of the following five steps.

Step 1 We use a family of positive operator-valued measurement (POVM) consisting of two operators given by $\sum_{i=0,1} m_i^\dagger m_i = I$ to obtain partial information on the state of the single-qubit system. The WM operators m_0 and m_1 are along the z-axis and defined as

$$m_0 = \begin{bmatrix} \cos(\omega/2) & 0 \\ 0 & \sin(\omega/2) \end{bmatrix},$$
$$m_1 = \begin{bmatrix} \sin(\omega/2) & 0 \\ 0 & \cos(\omega/2) \end{bmatrix}, \tag{1}$$

where $0 \le \omega \le \pi/2$ determines the strength of WMs. When $\omega = \pi/2$, the measurement does not change the state of the system; when $\omega = 0$, the measurement strength is at the highest amount and the measurement becomes a projection measurement; when $0 < \omega < \pi/2$, one can strike a balance between the desired information gain and the unwanted state disturbance. After applying pre-WMs in Eq. (1), the state of the system is described as

$$\rho_{m_i} = \frac{m_i \rho_{\rm in} m_i^\dagger}{{\rm tr}(m_i \rho_{\rm in} m_i^\dagger)} \tag{2}$$

with a probability

$$g_{m_i} = {\rm tr}(m_i \rho_{\rm in} m_i^\dagger), \tag{3}$$

where $\rho_{\rm in}$ is the unknown initial state of a single-qubit system.

Step 2 Feedforward operators f_0 and f_1 are used to transfer the system state to a state that is less vulnerable to the effects of FTTN and defined as

$$f_0 = \begin{bmatrix} 1 & 0 \\ 0 & 1 \end{bmatrix}, \quad f_1 = \begin{bmatrix} 0 & 1 \\ 1 & 0 \end{bmatrix}. \tag{4}$$

If the measurement result corresponding to m_0 is acquired, it means that the state of the single-qubit system is near the ground state and immune to the effects of the noise channel, hence the feedforward operator f_0 is selected as an identity operator; if the measurement result corresponding to m_1 is acquired, it means that the system state is close to the excited state, hence another feedforward operator f_1 is designed to transfer the system to a state that is immune to the effects of the noise channel.

After this step, the state of the system changes to $\rho_{f_i} = f_i \rho_{m_i} f_i^\dagger$ with a probability $g_{f_i} = g_{m_i}$.

Step 3 The single-qubit system passes through the FTTN channel and we apply EAM on the environment. The Kraus operators of the FTTN channel for the single-qubit system are defined as[42]

$$\begin{aligned} k_0 &= \begin{bmatrix} \sqrt{p} & 0 \\ 0 & \sqrt{p(1-r)} \end{bmatrix}, \quad k_1 = \begin{bmatrix} 0 & \sqrt{pr} \\ 0 & 0 \end{bmatrix}, \\ k_2 &= \begin{bmatrix} \sqrt{(1-p)(1-r)} & 0 \\ 0 & \sqrt{1-p} \end{bmatrix}, \\ k_3 &= \begin{bmatrix} 0 & 0 \\ \sqrt{r(1-p)} & 0 \end{bmatrix}, \end{aligned} \tag{5}$$

where $r \in [0,1]$ is the probability that the excited state decays to the ground state, $p = [1+\exp(-\omega_c/k_B T)]^{-1} (0.5 \le p \le 1)$ is a parameter related to the temperature of thermal bath, in which ω_c is the transition frequency, k_B is the Boltzmann constant, and T denotes the temperature. The definition of p reveals that it decreases as the temperature T increases.

The objective of applying EAM to the noise channel is to select only the results corresponding to invertible Kraus operators by measuring the environment (noise channel) coupled to the system of interest as well as to discard the other results. To be specific, a measurement is performed on the environment, which makes the environment collapse to the eigenstates of the measured observable, and the protected quantum system is projected onto a state related to the measurement outcome of the environment. If the noise channel collapses to the n^{th} eigenstate, the non-normalized density matrix of the protected quantum system becomes $\rho^n = K_n \rho K_n^\dagger$, where K_n is an invertible Kraus operator and ρ is the initial state of the protected quantum system. Obviously, only k_0 and k_2 in Eq. (5) are invertible. As a result, after this step, the state of the system changes to

$$\rho_{k_i} = \frac{k_0 \rho_{f_i} k_0^\dagger + k_2 \rho_{f_i} k_2^\dagger}{\text{tr}(k_0 \rho_{f_i} k_0^\dagger + k_2 \rho_{f_i} k_2^\dagger)} \tag{6}$$

with a probability

$$g_{k_i} = g_{f_i} \text{tr}(k_0 \rho_{f_i} k_0^\dagger + k_2 \rho_{f_i} k_2^\dagger). \tag{7}$$

Step 4 The corresponding reversed feedforward operator f_0^{-1} or f_1^{-1} is applied after the single-qubit system passes through the FTTN channel. Since both f_0 and f_1 are unitary matrices, $f_0^{-1} = f_0$ and $f_1^{-1} = f_1$ hold, i.e., the reversed feedforward operators are the same as the feedforward operators in Eq. (4). After this step, the state of the system changes to $\rho_{f_i^{-1}} = f_i \rho_{k_i} f_i^\dagger$ with a probability $g_{f_i^{-1}} = g_{k_i}$.

Step 5 Finally, the damped state is recovered to its initial state by using the post-WM operators mr_0 or mr_1, where $m_i \cdot mr_i$ is approximately equal to the identity matrix; mr_0 and mr_1 are selected from the complete measurement sets $\{mr_0, \overline{mr_0}\}$ and $\{mr_1, \overline{mr_1}\}$, respectively, i.e.,

$$\begin{aligned} mr_0 &= \begin{bmatrix} q & 0 \\ 0 & 1 \end{bmatrix}, \quad \overline{mr_0} = \begin{bmatrix} \sqrt{1-q^2} & 0 \\ 0 & 0 \end{bmatrix}, \\ mr_1 &= \begin{bmatrix} 1 & 0 \\ 0 & q \end{bmatrix}, \quad \overline{mr_1} = \begin{bmatrix} 0 & 0 \\ 0 & \sqrt{1-q^2} \end{bmatrix}, \end{aligned} \tag{8}$$

where $q \in [0,1]$ denotes the strength of the post-WMs. In our scheme, we only keep the results of mr_i, discard the results corresponding to $\overline{mr_i}$, and normalize the final state after applying the post-WM.

After the last step, the density matrix of the protected single-qubit system changes to

$$\rho_{mr_i} = \frac{mr_i \rho_{f_i^{-1}} mr_i^\dagger}{\text{tr}(mr_i \rho_{f_i^{-1}} mr_i^\dagger)} \tag{9}$$

with a probability

$$g_{mr_i} = g_{f_i^{-1}} \text{tr}(mr_i \rho_{f_i^{-1}} mr_i^\dagger). \tag{10}$$

Remark 1 Note that the proposed QFFC-EAM scheme works in a probabilistic manner, since the post-WM operators are incomplete and EAM cannot always be done successfully.

In a nutshell, the nonnormalized final states $\tilde{\rho}_{m_0}^{\text{fin}}$ and $\tilde{\rho}_{m_1}^{\text{fin}}$ corresponding to the WM operators m_0 and m_1 are calculated as

$$\begin{aligned} \tilde{\rho}_{m_0}^{\text{fin}} &= \sum_{i=0,2} (mr_0 f_0 k_i f_0 m_0) \rho_{\text{in}} (mr_0 f_0 k_i f_0 m_0)^\dagger, \\ \tilde{\rho}_{m_1}^{\text{fin}} &= \sum_{i=0,2} (mr_1 f_1 k_i f_1 m_1) \rho_{\text{in}} (mr_1 f_1 k_i f_1 m_1)^\dagger, \end{aligned} \tag{11}$$

with the corresponding success probabilities $g_{m_0}^{(1)}$ and $g_{m_1}^{(1)}$ as

$$g_{m_0}^{(1)} = \text{tr}(\tilde{\rho}_{m_0}^{\text{fin}}), \quad g_{m_1}^{(1)} = \text{tr}(\tilde{\rho}_{m_1}^{\text{fin}}). \tag{12}$$

Therefore, the normalized final states $\rho_{m_0}^{\text{fin}}$ and $\rho_{m_1}^{\text{fin}}$ corresponding to m_0 and m_1 are

$$\rho_{m_0}^{\text{fin}} = \frac{\tilde{\rho}_{m_0}^{\text{fin}}}{g_{m_0}}, \quad \rho_{m_1}^{\text{fin}} = \frac{\tilde{\rho}_{m_1}^{\text{fin}}}{g_{m_1}}. \tag{13}$$

To quantify the performance of QFFC-EAM scheme, fidelity is used to measure the similarity between the final state and the initial state and defined as

$$\mathrm{fid}_{m_i}^{(1)} = \left[\mathrm{tr}\left(\sqrt{\sqrt{\rho_{m_i}^{\mathrm{fin}}}\rho_{\mathrm{in}}\sqrt{\rho_{m_i}^{\mathrm{fin}}}}\right)\right]^2. \tag{14}$$

For the sake of avoiding calculating the square root of a matrix, we define the fidelity for pure and mixed initial states as follows.

When the initial state is a pure state $|\psi_{\mathrm{in}}\rangle$, the fidelity in Eq. (14) is equivalent to[43]

$$\mathrm{fid}_{m_i}^{(1)} = \langle\psi_{\mathrm{in}}|\rho_{m_i}^{\mathrm{fin}}|\psi_{\mathrm{in}}\rangle = \mathrm{tr}(\rho_{m_i}^{\mathrm{fin}}\rho_{\mathrm{in}}). \tag{15}$$

When the initial state is a mixed state, the fidelity in Eq. (14) can be expressed as[44]

$$\mathrm{fid}_{m_i}^{(1)} = \mathrm{tr}(\rho_{m_i}^{\mathrm{fin}}\rho_{\mathrm{in}}) + 2\sqrt{\det(\rho_{m_i}^{\mathrm{fin}}\rho_{\mathrm{in}})}, \tag{16}$$

where $\det(\cdot)$ denotes the matrix determinant.

The total fidelity $\mathrm{fid}_{\mathrm{total}}^{(1)}$ and total success probability $g_{\mathrm{total}}^{(1)}$ of the QFFC-EAM scheme are calculated as

$$\mathrm{fid}_{\mathrm{total}}^{(1)} = \frac{g_{m_0}^{(1)}\mathrm{fid}_{m_0}^{(1)} + g_{m_1}^{(1)}\mathrm{fid}_{m_1}^{(1)}}{g_{m_0}^{(1)} + g_{m_1}^{(1)}},$$

$$g_{\mathrm{total}}^{(1)} = g_{m_0}^{(1)} + g_{m_1}^{(1)}. \tag{17}$$

Suppose that the initial state is an arbitrary single-qubit pure state $|\psi_{\mathrm{in}}\rangle = a|0\rangle + b|1\rangle$, where $|a|^2 + |b|^2 = 1$ and $a, b \in \mathbb{C}$. The total fidelity of the QFFC-EAM scheme is calculated as

$$\begin{aligned}\mathrm{fid}_{\mathrm{total}}^{(1)} &= 1+2|b|^4-2|b|^2 \\ &\quad + \frac{4q\left(|b|^2-|b|^4\right)\tan(\omega/2)\sqrt{1-r}}{q^2(1+pr-r)+(1-pr)\tan^2(\omega/2)}\end{aligned} \tag{18}$$

with the total success probability

$$g_{\mathrm{total}}^{(1)} = (1-pr)\sin^2(\omega/2) + q^2(1+pr-r)\cos^2(\omega/2). \tag{19}$$

According to Eq. (19), the total success probability is independent of the initial state, while the total fidelity in Eq. (18) is dependent on the initial state. In Fig. 2, we depict the total fidelity $\mathrm{fid}_{\mathrm{total}}^{(1)}$ vs. ω and q by fixing $p = 0.9$ and $r = 0.6$, and setting the initial state parameter $|b|$ to be 0.3, 0.5, 0.7 and 0.9, respectively.

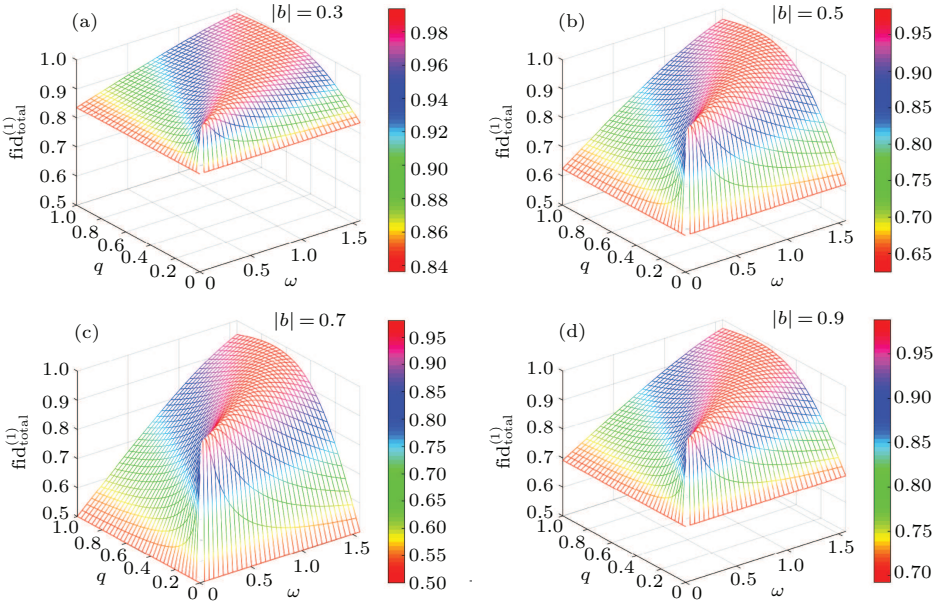


Fig. 2. Total fidelity vs. ω and q. Here $p = 0.9$ and $r = 0.6$.

Two key conclusions can be drawn from Fig. 2. On the one hand, the total fidelity of the protection scheme varies considerably with different initial states. If the other parameters are fixed, the total fidelity reaches the minimum value when $|b|^2 = 1/2$, and is at a high level when $|b|^2$ is close to 0 or 1. What's more, the regions corresponding to a high fidelity in Figs. 2(a) and 2(d) are significantly larger than those in Figs. 2(b) and 2(c). On the other hand, for a certain initial state, the maximum total fidelity depends on the values of ω and q.

According to the first conclusion, it is needed to define the average fidelity for all possible initial states to evaluate the performance of the QFFC-EAM scheme as

$$\mathrm{fid}_{\mathrm{av}}^{(1)} = \int \mathrm{d}\psi \quad \mathrm{fid}_{\mathrm{total}}^{(1)}. \tag{20}$$

Therefore, the analytical expression of $\mathrm{fid}_{\mathrm{av}}^{(1)}$ is obtained as

$$\mathrm{fid}_{\mathrm{av}}^{(1)} = \frac{11}{15} + \frac{8q\tan(\omega/2)\sqrt{1-r}}{15[q^2(1+pr-r)+(1-pr)\tan^2(\omega/2)]}. \tag{21}$$

The average fidelity $\mathrm{fid}_{\mathrm{av}}^{(1)}$ and the corresponding total success probability $g_{\mathrm{total}}^{(1)}$ vs. ω and q are depicted in Figs. 3(a) and 3(b), respectively.

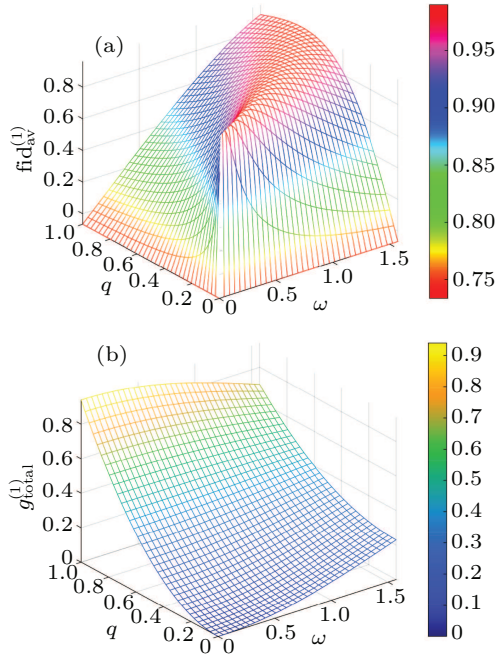


Fig. 3. (a) Average fidelity $\mathrm{fid}_{\mathrm{av}}^{(1)}$ vs. ω and q. (b) Total success probability $g_{\mathrm{total}}^{(1)}$ vs. ω and q. Here $p = 0.9$, $r = 0.6$.

The second conclusion inspires us to find out the optimal relationship between the pre-WM strength ω and the post-WM strength q to maximize the total fidelity. By calculating the partial derivative of $\mathrm{fid}_{\mathrm{total}}^{(1)}$ with respect to q, the following relationship among q, ω, p, and r is deduced to achieve the maximum total fidelity (see Appendix A for proof):

$$q_{\mathrm{opt}} = \tan(\omega/2)\sqrt{\frac{1-pr}{1+pr-r}}. \tag{22}$$

From now on, we call Eq. (22) as the optimal condition of the fidelity, which is independent of the initial state. Hence, even if the initial state is unknown, the maximum total fidelity can be achieved as long as q satisfies Eq. (22). Under the optimal condition, the total fidelity of the proposed QFFC-EAM scheme becomes

$$\mathrm{fid}_{\mathrm{total}}^{(1)^{\mathrm{opt}}} = 1 + 2|b|^4 - 2|b|^2 + \frac{2(|b|^2 - |b|^4)\sqrt{1-r}}{\sqrt{1-pr}\sqrt{1+pr-r}} \tag{23}$$

with the corresponding total success probability

$$g_{\mathrm{total}}^{(1)^{\mathrm{opt}}} = 2(1-pr)\sin^2(\omega/2). \tag{24}$$

Moreover, the maximum average fidelity of the QFFC-EAM scheme is calculated as

$$\mathrm{fid}_{\mathrm{av}}^{(1)^{\mathrm{opt}}} = \frac{11}{15} + \frac{4\sqrt{1-r}}{15\sqrt{1-pr}\sqrt{1+pr-r}}. \tag{25}$$

Importantly, by considering the optimal condition in Eq. (22), it is found that the total and the average fidelities are independent of ω, while the success probability is still dependent on ω. Hence, the maximum success probability can be obtained by only adjusting ω without affecting the value of fidelity, which has barely occurred in previous studies. In fact, in almost all of the previous WM based protection schemes, there is a trade-off between the fidelity and the success probability, in which the fidelity is promoted at the expense of the success probability, and vice versa; see, e.g., Refs. [32–37]. While in our proposed QFFC-EAM scheme the fidelity and the success probability can be optimized separately without affecting each other. According to Eq. (24), it is clear that the optimum value of ω in the sense of maximizing the total success probability is

$$\omega_{\mathrm{opt}} = \pi/2. \tag{26}$$

And the maximum total success probability under ω_{opt} is

$$g_{\mathrm{total}}^{(1)^{\mathrm{opt}}} = 1 - pr. \tag{27}$$

The maximum average fidelity $\mathrm{fid}_{\mathrm{av}}^{(1)^{\mathrm{opt}}}$ and the corresponding maximum total success probability $g_{\mathrm{total}}^{(1)^{\mathrm{opt}}}$ vs. p and r under q_{opt} and ω_{opt} are depicted in Figs. 4(a) and 4(b), respectively.

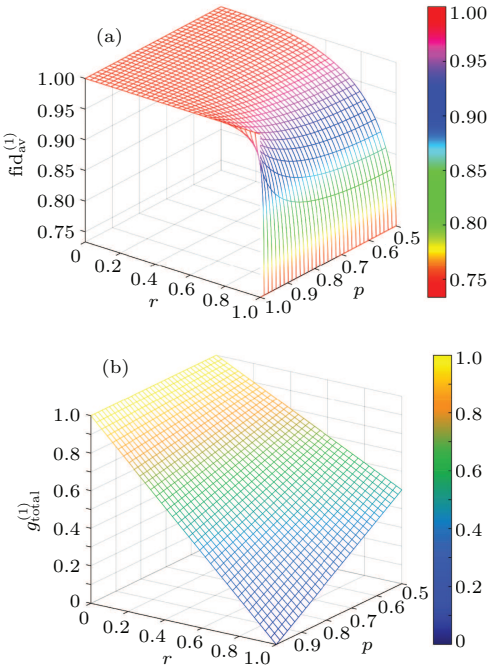


Fig. 4. (a) Maximum average fidelity $\mathrm{fid}_{\mathrm{av}}^{(1)^{\mathrm{opt}}}$ vs. p and r. (b) Maximum total success probability vs. p and r.

As shown in Fig. 5(a), to observe the effect of each step in the QFFC-EAM scheme intuitively, we study a single-qubit pure state protection on the Bloch sphere, where the initial state is selected as $|\psi\rangle = \cos(5\pi/8)|0\rangle + \sin(5\pi/8)\mathrm{e}^{-\pi/6}|1\rangle$, the parameters of the FTTN channel are set as $p = 0.95$ and $r = 0.7$, the pre-WM strength ω is set to be $\pi/4$, and the post-WM strength q is set to its optimum value in Eq. (22)

to maximize the fidelity. Specifically, the red arrow indicates the initial state, the black arrow indicates the state after the pre-WM operator, the blue arrow indicates the state after the feedforward operator, the cyan arrow indicates the state after the FTTN channel, the yellow arrow indicates the state after the reversed feedforward operator, and the green arrow indicates the final state after the post-WM operator. For comparison, we also study the case under no protection in Fig. 5(b), where the red arrow indicates the same initial state as that in Fig. 5(a), and the cyan arrow indicates the final state after the same FTTN channel under no protection.

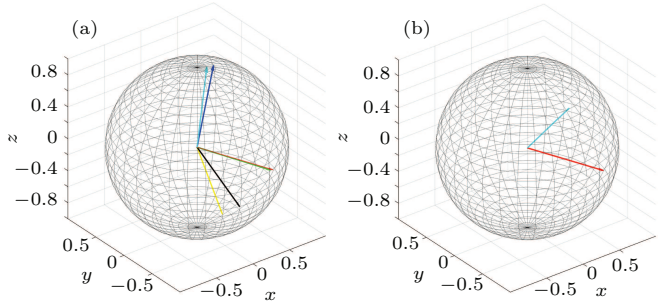


Fig. 5. (a) State evolution of the protected single-qubit pure state after each step of QFFC-EAM. (b) State evolution of the single-qubit pure state under no protection.

Next, let us quantify the fidelity improvement of the proposed QFFC-EAM scheme. In the scheme under no protection, the damping final state is

$$\rho_{\mathrm{FTTN}}^{\mathrm{fin}} = \sum_{i=0}^{3} k_i \rho_{\mathrm{in}} k_i^{\dagger}, \tag{28}$$

where k_i are the Kraus operators in Eq. (5).

Therefore, the fidelity of the unprotected scheme is calculated as

$$\begin{aligned} \mathrm{fid}_{\mathrm{FTTN}}^{(1)} &= \left[\mathrm{tr}\left(\sqrt{\sqrt{\rho_{\mathrm{FTTN}}^{\mathrm{fin}}}\rho_{\mathrm{in}}\sqrt{\rho_{\mathrm{FTTN}}^{\mathrm{fin}}}}\right)\right]^2 \\ &= 1+pr-r-|b|^2(2pr-3r+2) \\ &\quad -|b|^4(2r-2)+2(|b|^2-|b|^4)\sqrt{1-r}. \end{aligned} \tag{29}$$

By adopting the optimal condition of fidelity in Eq. (22), the improvement of the total fidelity is defined as

$$\begin{aligned} \mathrm{fid}_{\mathrm{improve}}^{(1)} &= \mathrm{fid}_{\mathrm{total}}^{(1)^{\mathrm{opt}}} - \mathrm{fid}_{\mathrm{FTTN}}^{(1)} \\ &= 2|b|^4-2|b|^2-pr+r \\ &\quad +|b|^2(2pr-3r+2)+|b|^4(2r-2) \\ &\quad -2(|b|^2-|b|^4)\sqrt{1-r} \\ &\quad +\frac{2(|b|^2-|b|^4)\sqrt{1-r}}{\sqrt{1-pr}\sqrt{1+pr-r}}. \end{aligned} \tag{30}$$

Figure 6 illustrates that $\mathrm{fid}_{\mathrm{improve}}^{(1)}$ is a function of $|b|$ and r under a fixed value of p, where the total fidelity is improved for arbitrary initial states. Moreover, $\mathrm{fid}_{\mathrm{improve}}^{(1)}$ rises with the increase of $|b|$, since the closer $|b|$ is to 1, the closer the system state is to the excited state and the more vulnerable it is to the effects of the noise channel. Additionally, in high damping cases ($r > 0.8$), the fidelity improvement is particularly obvious, which demonstrates the effectiveness of our proposed scheme.

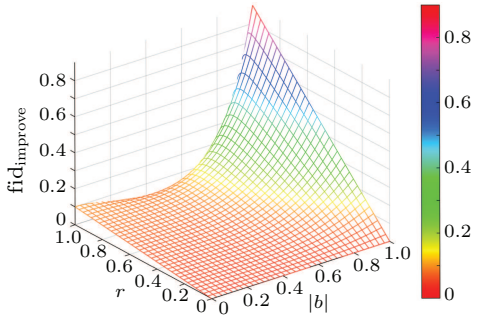


Fig. 6. $\mathrm{fid}_{\mathrm{improve}}^{(1)}$ vs. $|b|$ and r, for $p = 0.9$.

For further comparison, we consider the QFFC scheme in Ref. [41] to highlight the superiority of our proposed QFFC-EAM scheme, and the maximum fidelity improvements of the two schemes are shown in Fig. 7. Same as the control objective of our proposed QFFC-EAM, the QFFC scheme in Ref. [41] was designed to deal with quantum systems subject to FTTN; however, it does not apply EAM, and uses the rotation operator to replace the post-WM operator in the last step.

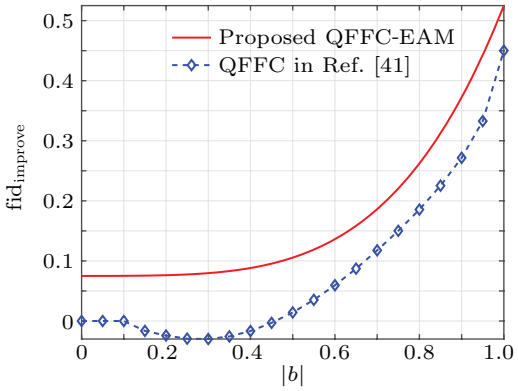


Fig. 7. Comparisons between the proposed QFFC-EAM and the QFFC in Ref. [41]. Here $p = 0.95$ and $r = 0.5$.

To plot Fig. 7, analytical expressions of maximum fidelity improvements of the proposed QFFC-EAM are deduced, while the maximum fidelity improvement of the QFFC scheme in Ref. [41] is obtained in a numerical way. As demonstrated in Fig. 7, our proposed QFFC-EAM scheme outperforms the QFFC scheme in Ref. [41] for all possible initial states. The underlying reason for this is that the EAM gains more knowledge about the noise channel which helps us to select the states corresponding to invertible Kraus operators. Moreover, compared to the unitary rotations utilized in the QFFC scheme in Ref. [41], we achieve a higher fidelity in the QFFC-EAM scheme by using post-WM after EAM.

Remark 2 Note that the initial state of the protected single-qubit system is allowed to be totally unknown in our proposed QFFC-EAM scheme, while the QFFC scheme in Ref. [41] cannot achieve the maximum totally fidelity if the prior information on the initial state is not available.

3. Application to controlled quantum teleportation

Controlled quantum teleportation is an important branch of quantum communication,[45] where the receiver can gain the information on the teleported qubit from the sender only with the permission of the controller. In this section, we apply the QFFC-EAM scheme to the protection of controlled quantum teleportation through two independent FTTN channels. We assume that a third party (Charlie) works as the controller, and prepares a Bell state $|\psi\rangle_{\rm ab}=\frac{1}{\sqrt{2}}(|00\rangle+|11\rangle)$ as the shared entanglement and sends the first qubit to Alice and the second qubit to Bob through an FTTN channel, respectively.

In order to develop high-fidelity quantum teleportation schemes, a feasible solution is to use the proposed QFFC-EAM to protect the shared entanglement against decoherence and then implement an original quantum teleportation protocol. In Section 2, we have illustrated the protection of a single-qubit state from FTTN. Since the Bell state is a two-qubit state, the operators in each step should be reconstructed. For simplicity, we assume that each qubit goes through an FTTN channel, and all parameters of the two FTTN channels are the same. The 4×4 operators of the two-qubit case can be constructed by using the tensor product as follows.

The two-qubit pre-WM operators are constructed as

$$\begin{aligned} &M_0=m_0\otimes m_0, \quad M_1=m_0\otimes m_1,\\ &M_2=m_1\otimes m_0, \quad M_3=m_1\otimes m_1 \end{aligned} \tag{31}$$

with corresponding feedforward operators

$$\begin{aligned} &F_0=f_0\otimes f_0, \quad F_1=f_0\otimes f_1,\\ &F_2=f_1\otimes f_0, \quad F_3=f_1\otimes f_1. \end{aligned} \tag{32}$$

The invertible Kraus operators of the FTTN channel are constructed as

$$\begin{aligned} &K_0=k_0\otimes k_0, \quad K_1=k_0\otimes k_2,\\ &K_2=k_2\otimes k_0, \quad K_3=k_2\otimes k_2. \end{aligned} \tag{33}$$

Remark 3 There are 16 Kraus operators in total to characterize the two independent FTTN channels, but only the quantum trajectories corresponding to the invertible Kraus operators are kept due to the principle of EAM; hence we only present the four invertible Kraus operators for simplicity.

The reversed feedforward operators are the same as those in Eq. (32) since f_i $(i=0,1)$ are unitary matrices, i.e., $(f_i\otimes f_j)^{-1}=f_i^{-1}\otimes f_j^{-1}=f_i\otimes f_j$, where $i,j=0,1$.

The two-qubit post-WM operators are constructed as

$$\begin{aligned} &MR_0=mr_0\otimes mr_0, \quad MR_1=mr_0\otimes mr_1,\\ &MR_2=mr_1\otimes mr_0, \quad MR_3=mr_1\otimes mr_1. \end{aligned} \tag{34}$$

In the entanglement distribution process of the controlled quantum teleportation, Charlie applies the pre-WM and the feedforward control to the first and the second qubit of the entangled pair, respectively, before the two qubits pass through the FTTN channel, then Alice and Bob performs a measurement on the coupled environment and keep the results corresponding to invertible Kraus operators when their qubit is in the FTTN channel, finally they apply the reversed feedforward control and the post-WM to their qubit. The schematic diagram of the protected controlled quantum teleportation through two independent FTTN channels is shown in Fig. 8.

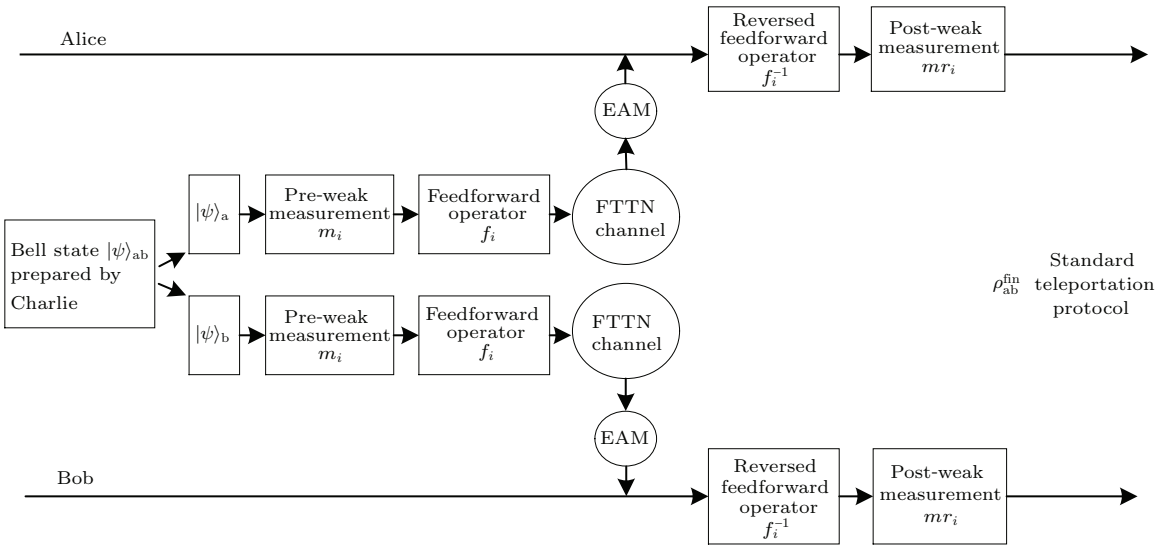


Fig. 8. Schematic diagram of the protected controlled quantum teleportation through two independent FTTN channels.

By analyzing the protection of the shared entanglement step by step, we found that if the measurement result corresponding to M_1 or M_2 is obtained, the final state is the same whether the post-WM operators MR_1 or MR_2 is applied or not. In other words, in these cases, the post-WM operators are not necessary. In addition, a higher success probability can be achieved by removing the unnecessary post-WM; however, if the measurement results corresponding to M_0 and M_3 are obtained, the post-WM is still necessary (see an illustrative example in Appendix B for details).

Therefore, for cases corresponding to M_1 and M_2, the final state ρ_{M_j} is calculated as

$$\rho_{M_j} = \frac{\sum_{i=0}^{3} F_j K_i F_j M_j \rho_{\rm ab} (F_j K_i F_j M_j)^\dagger}{\mathrm{tr}\Big[\sum_{i=0}^{3} F_j K_i F_j M_j \rho_{\rm ab} (F_j K_i F_j M_j)^\dagger\Big]} \tag{35}$$

with corresponding success probability g_{M_j} as

$$g_{M_j} = \mathrm{tr}\Big[\sum_{i=0}^{3} F_j K_i F_j M_j \rho_{\rm ab} (F_j K_i F_j M_j)^\dagger\Big], \tag{36}$$

where $\rho_{\rm ab} = |\psi_{\rm ab}\rangle\langle\psi_{\rm ab}|$ is the density matrix of the Bell state.

Likewise, for cases corresponding to M_0 and M_3, the final state ρ_{M_k} is calculated as

$$\rho_{M_k} = \frac{\sum_{i=0}^{3} MR_k F_k K_i F_k M_k \rho_{\rm ab} (MR_k F_k K_i F_k M_k)^\dagger}{\mathrm{tr}\Big[\sum_{i=0}^{3} MR_k F_k K_i F_k M_k \rho_{\rm ab} (MR_k F_k K_i F_k M_k)^\dagger\Big]} \tag{37}$$

with corresponding success probability g_{M_k} as

$$g_{M_k} = \mathrm{tr}\Big[\sum_{i=0}^{3} MR_k F_k K_i F_k M_k \rho_{\rm ab} (MR_k F_k K_i F_k M_k)^\dagger\Big]. \tag{38}$$

Hence, by considering the optimal condition of the fidelity in Eq. (22), the total fidelity of the protected Bell state is calculated as

$$\mathrm{fid}_{\rm Bell}^{\rm opt} = \frac{\sum_{i=0}^{3} g_{M_i} \mathrm{fid}_{M_i}}{\sum_{i=0}^{3} g_{M_i}} = \frac{1}{2} + \frac{1-r}{2(1-pr)(1+pr-r)} \tag{39}$$

with the total success probability as

$$g_{\rm ab}^{\rm fin^{opt}} = \frac{\sin^2(\omega)(1-pr)(1+pr-r)}{2} + 2\sin^4(\omega/2)(1-pr)^2, \tag{40}$$

where $\mathrm{fid}_{M_i} = \mathrm{tr}(\rho_{M_i}\rho_{\rm ab})$ are fidelities corresponding to different M_i.

It is known that the average teleportation fidelity directly depends on the fidelity of the shared entanglement; hence, it is necessary to study the total fidelity of the Bell state after the QFFC-EAM scheme is applied. The total fidelity of the protected Bell state in Eq. (39) vs. p and r under the optimal condition of the fidelity in Eq. (22) is depicted in Fig. 9(a), and the unprotected scenario is depicted in Fig. 9(b) for comparison.

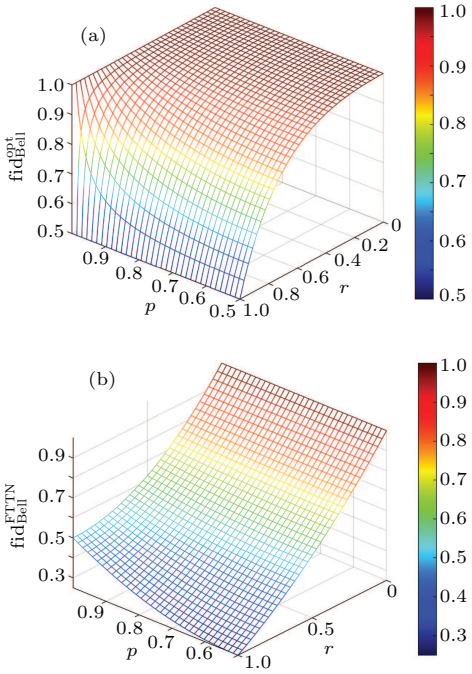


Fig. 9. (a) Total fidelity of the protected Bell state vs. p and r. (b) Total fidelity of the Bell state vs. p and r under no protection.

After a successful entanglement distribution, we carry out the standard quantum teleportation protocol. The density matrix of the unknown input state that Alice wishes to teleport to Bob is described as

$$\rho_{\rm in} = \begin{bmatrix} |a|^2 & ab^* \\ a^*b & |b|^2 \end{bmatrix}, \tag{41}$$

where the superscript $*$ denotes complex conjugation. After the standard teleportation protocol, the state of Bob's qubit becomes (see Appendix C for the specific calculation process)

$$\rho_{\rm out} = \begin{bmatrix} |a|^2 & \sigma ab^* \\ \sigma a^*b & |b|^2 \end{bmatrix}, \tag{42}$$

where

$$\sigma = \frac{q^2\sin^2(\omega)(1-r)}{[\sin^2(\omega/2)(1-pr) + q^2\cos^2(\omega/2)(1+pr-r)]^2}.$$

Under the optimal condition of the fidelity in Eq. (22), the state of Bob's qubit is described as

$$\rho_{\rm out}^{\rm opt} = \begin{bmatrix} |a|^2 & \frac{ab^*(1-r)}{(1-pr)(1+pr-r)} \\ \frac{a^*b(1-r)}{(1-pr)(1+pr-r)} & |b|^2 \end{bmatrix}. \tag{43}$$

In order to evaluate the performance of the protected quantum teleportation, the average fidelity between the input state $\rho_{\rm in}$ and the output state $\rho_{\rm out}^{\rm opt}$ is calculated as

$$\mathrm{fid}_{\rm protect}^{\rm av} = \int \mathrm{d}\psi \langle\psi_{\rm in}|\rho_{\rm out}|\psi_{\rm in}\rangle = \frac{11}{15} + \frac{4\sigma}{15}. \tag{44}$$

Additionally, the maximum average fidelity is calculated as

$$\begin{aligned}\mathrm{fid}_{\mathrm{protect}}^{\mathrm{av^{opt}}} &= \int \mathrm{d}\psi \langle\psi_{\mathrm{in}}|\rho_{\mathrm{out}}^{\mathrm{opt}}|\psi_{\mathrm{in}}\rangle \\ &= \frac{11}{15} + \frac{4(1-r)}{15(1-pr)(1+pr-r)}. \end{aligned} \tag{45}$$

For comparison, we consider the original quantum teleportation under no protection. Similarly, the average fidelity of quantum teleportation under no protection is obtained as

$$\mathrm{fid}_{\mathrm{FTTN}}^{\mathrm{av}} = 1 + \frac{14p^2r^2 - 14pr^2 + 7r^2 - 11r}{15}. \tag{46}$$

To quantify the performance of the proposed scheme, the improvement of the average teleportation fidelity is defined as

$$\begin{aligned}\mathrm{fid}_{\mathrm{improve}}^{\mathrm{av}} &= \mathrm{fid}_{\mathrm{protect}}^{\mathrm{av^{opt}}} - \mathrm{fid}_{\mathrm{FTTN}}^{\mathrm{av}} \\ &= \frac{4(1-r)}{15(1-pr)(1+pr-r)} \\ &\quad - \frac{14p^2r^2 - 14pr^2 + 7r^2 - 11r + 4}{15}. \end{aligned} \tag{47}$$

Furthermore, we plot $\mathrm{fid}_{\mathrm{improve}}^{\mathrm{av}}$ vs. p and r in Fig. 10, from which one can see that a higher average teleportation fidelity can be always achieved by applying the QFFC-EAM to the shared entanglement.

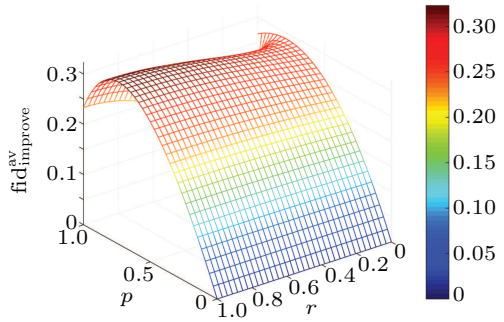


Fig. 10. The $\mathrm{fid}_{\mathrm{improve}}^{\mathrm{av}}$ vs. p and r.

Remark 4 The feasible applications of the proposed QFFC-EAM are not limited to the protection of the controlled quantum teleportation. Note that in Fig. 8, the focus is on protecting the shared entanglement during the entanglement distribution process, and the original quantum teleportation protocol does not need modifying. Hence, QFFC-EAM can also be successfully applied to protecting other entanglement-based quantum communications, e.g., quantum secret sharing and quantum key distribution.

4. Conclusion

In summary, we have proposed a quantum state protection scheme via QFFC combined with EAM to protect arbitrary unknown initial states from FTTN. It is verified that there exists no trade-off between the fidelity and the success probability in our proposed scheme, which was rarely reported in previous studies. By finding out the optimum strengths of the pre- and post-WMs, the fidelity and the success probability are maximized separately. Analytical expressions of the maximum fidelity and the maximum total success probability are derived. Performance of the proposed scheme is comprehensively analyzed by choosing various WM strengths and decoherence parameters in a series of simulation studies. For comparison, the unprotected scenario and the QFFC scheme in Ref. [41] are considered to demonstrate the superiority of our proposed scheme. Furthermore, it is shown that the proposed scheme has a promising prospect in quantum teleportation through noise channels. More importantly, we believe that the proposed scheme can also play a role in protecting other entanglement-based quantum communications.

Appendix A

Here, the proof of the optimal condition in the sense of maximizing the total fidelity is given. All parameters except ω and q are regarded as constants. First, let us introduce the following notations:

$$\begin{aligned} &u_1 = 4\tan(\omega/2)\sqrt{1-r},\ \ u_2 = 1+pr-r, \\ &u_3 = (1-pr)\tan^2(\omega/2),\ \ u_4 = |b|^2 - |b|^4, \end{aligned} \tag{A1}$$

where u_1, u_2, u_3, and u_4 are all non-negative since $\omega \in [0,\pi/2]$, $r \in [0,1]$, $p \in [0.5,1]$, and $|b| \in [0,1]$ hold.

By using the notations in Eq. (A1), the total fidelity in Eq. (18) can be re-expressed as

$$\mathrm{fid}_{\mathrm{total}}^{(1)} = -2u_4 + \frac{u_1u_4q}{u_2q^2+u_3}. \tag{A2}$$

Then, the partial derivative of $\mathrm{fid}_{\mathrm{total}}^{(1)}$ with respect to q is calculated as

$$\frac{\partial \mathrm{fid}_{\mathrm{total}}^{(1)}}{\partial q} = \frac{u_1u_4(u_3-k_2q^2)}{(u_2q^2+u_3)^2}. \tag{A3}$$

To find out the optimum q, we set the partial derivative to be 0. Considering that the value of q is between 0 and 1, we ignore the negative values and obtain

$$q = \sqrt{\frac{u_3}{u_2}} = \tan(\omega/2)\sqrt{\frac{1-pr}{1+pr-r}}. \tag{A4}$$

Since $0 \le \tan(\omega/2) \le 1$ and $(1+pr-r) \ge (1-pr)$ hold, the value of q in Eq. (A4) is between 0 and 1, and the value of the above partial derivative is greater than 0 within the interval $(0,q)$ and less than 0 within the interval $(q,1)$. Hence, the maximum value of $\mathrm{fid}_{\mathrm{total}}^{(1)}$ is reached for any fixed $\omega \in [0,\pi/2]$ if Eq. (A4) is satisfied. In addition, substituting q in Eq. (A4) into the analytical expression of the total fidelity, one obtains a constant which is independent of ω and q. Hence, it is concluded that the total fidelity is maximized when the relationship in Eq. (A4) holds. This completes the proof.

Appendix B

Here, we show that the post-WM operator is not always necessary. Without loss of generality, we assume that the measurement result corresponding to M_1 is obtained, and the reversed feedforward operator F_1 is applied. In this step, the state of the shared entanglement is calculated as

$$\rho_{F_1^{-1}} = \frac{\sum_{i=0}^{3} F_1K_iF_1M_1\rho_{\rm ab}(F_1K_iF_1M_1)^\dagger}{{\rm tr}[\sum_{i=0}^{3} F_1K_iF_1M_1\rho_{\rm ab}(F_1K_iF_1M_1)^\dagger]} = \begin{bmatrix} \frac{1}{2} & 0\ 0 & \frac{1-r}{2(1-pr)(1+pr-r)} \\ 0 & 0\ 0 & 0 \\ 0 & 0\ 0 & 0 \\ \frac{1-r}{2(1-pr)(1+pr-r)} & 0\ 0 & \frac{1}{2} \end{bmatrix} \tag{B1}$$

with the corresponding success probability

$$g_{F_1^{-1}} = {\rm tr}[\sum_{i=0}^{3} F_1K_iF_1M_1\rho_{\rm ab}(F_1K_iF_1M_1)^\dagger] = \frac{\sin^2(\omega)(1-pr)(1+pr-r)}{4}. \tag{B2}$$

Finally, after the post-WM, the state of the shared entanglement changes to

$$\rho_{MR_1} = \frac{MR_1\rho_{F_1^{-1}}MR_1{}^\dagger}{{\rm tr}(MR_1\rho_{F_1^{-1}}MR_1{}^\dagger)} = \begin{bmatrix} \frac{1}{2} & 0\ 0 & \frac{1-r}{2(1-pr)(1+pr-r)} \\ 0 & 0\ 0 & 0 \\ 0 & 0\ 0 & 0 \\ \frac{1-r}{2(1-pr)(1+pr-r)} & 0\ 0 & \frac{1}{2} \end{bmatrix} \tag{B3}$$

with the corresponding success probability

$$g_{MR_1} = g_{F_1^{-1}}{\rm tr}(MR_1\rho_{F_1^{-1}}MR_1{}^\dagger) = \frac{q^2\sin^2(\omega)(1-pr)(1+pr-r)}{4}. \tag{B4}$$

It can be seen from Eqs. (B1) and (B3) that $\rho_{F_1^{-1}} = \rho_{MR_1}$. Additionally, it can be seen from Eqs. (B2) and (B4) that the post-WM operator reduces the success probability of the protection scheme; hence, it is concluded that the post-WM operator is not necessary if the measurement result corresponding to M_1 is obtained. If the other measurement result corresponding to M_0, M_2 or M_3 is obtained, one can use the same method to analyze whether the post-WM can be removed or not. The remaining three cases will not be discussed due to similarity.

Appendix C

Here, we calculate the average teleportation fidelity under the optimal condition of the fidelity in Eq. (22). First, Alice interacts the input qubit with her half of the entangled pair. Hence, the state of the combined system consisting of the input qubit and her half of the entangled pair is

$$\rho_1 = \rho_{\rm in}\otimes\rho_{\rm ab}^{\rm fin} = \frac{1}{2}\begin{bmatrix} \alpha_2 & 0\ 0 & \alpha_1\alpha_2 & \alpha_5 & 0\ 0 & \alpha_1\alpha_5 \\ 0 & 0\ 0 & 0 & 0 & 0\ 0 & 0 \\ 0 & 0\ 0 & 0 & 0 & 0\ 0 & 0 \\ \alpha_1\alpha_2 & 0\ 0 & 0 & \alpha_1\alpha_5 & 0\ 0 & \alpha_5 \\ \alpha_4 & 0\ 0 & \alpha_1\alpha_4 & 0 & 0\ 0 & \alpha_1\alpha_3 \\ 0 & 0\ 0 & 0 & 0 & 0\ 0 & 0 \\ 0 & 0\ 0 & 0 & 0 & 0\ 0 & 0 \\ \alpha_1\alpha_4 & 0\ 0 & \alpha_4 & \alpha_1\alpha_3 & 0\ 0 & \alpha_3 \end{bmatrix}, \tag{C1}$$

where $\alpha_1 = \frac{1-r}{(1-pr)(1+pr-r)}$, $\alpha_2 = |a|^2$, $\alpha_3 = |b|^2$, $\alpha_4 = a^*b$, and $\alpha_5 = ab^*$.

Then, Alice applies a Bell joint measurement on the input qubit and her half of the protected entanglement under the basis $B_i = |b_i\rangle\langle b_i|\otimes I$ with I being the 2×2 identity matrix, and $|b_i\rangle$ are defined as

$$|b_1\rangle = \frac{1}{\sqrt{2}}(|00\rangle+|11\rangle),\ \ |b_2\rangle = \frac{1}{\sqrt{2}}(|00\rangle-|11\rangle),$$
$$|b_3\rangle = \frac{1}{\sqrt{2}}(|01\rangle+|10\rangle),\ \ |b_4\rangle = \frac{1}{\sqrt{2}}(|01\rangle-|10\rangle). \tag{C2}$$

After the Bell joint measurement, the state of Bob's qubit becomes

$$\rho_{B_i} = \frac{{\rm tr}_{12}(B_i\rho_1B_i)}{g_{B_i}}, \tag{C3}$$

where ${\rm tr}_{12}(\cdot)$ denotes the partial trace over the combined system consisting of the input qubit and Alice's half of the entangled pair, and $g_{B_i} = {\rm tr}(B_i\rho_1B_i)$ are the success probabilities corresponding to B_i.

Next, Alice informs Bob which result was obtained through a classical channel, and Bob applies a corresponding unitary operator according to Alice's measurement result. The unitary operators for each measurement result are

$$C_1 = I,\ \ C_2 = \sigma_z,\ \ C_3 = \sigma_x,\ \ C_4 = \sigma_z\sigma_x, \tag{C4}$$

where $\sigma_x = [0,1;1,0]$ and $\sigma_z = [1,0;0,-1]$ are Pauli operators.

Hence, the final output state of Bob's qubit is

$$\rho_{C_i} = C_i\rho_{B_i}C_i^\dagger = \begin{bmatrix} |a|^2 & \frac{ab^*(1-r)}{(1-pr)(1+pr-r)} \\ \frac{a^*b(1-r)}{(1-pr)(1+pr-r)} & |b|^2 \end{bmatrix}. \tag{C5}$$

The corresponding fidelity for each measurement result is defined as

$${\rm fid}_i = {\rm tr}(\rho_{C_i}\rho_{\rm in}). \tag{C6}$$

Therefore, the average teleportation fidelity is obtained as

$${\rm fid}_{\rm protect}^{\rm av} = \int {\rm d}\psi \sum_i g_{B_i}{\rm fid}_i$$

$$= \frac{11}{15} + \frac{4(1-r)}{15(1-pr)(1+pr-r)}. \tag{C7}$$

The calculation of the average teleportation fidelity under no protection is similar to the above process, and the result is given in Eq. (46).

Acknowledgements

Project supported by the National Natural Science Foundation of China (Grant No. 61973290), and a Program from Ministry of Science and Technology of China (Grant No. QN2022200007L).

References

[1] Cong S and Kuang S 2020 *Control Theory and Methods of Quantum Systems* (Hefei: University of Science and Technology of China Press) pp. 32–33 (in Chinese)
[2] Diamanti E, Lo H, Qi B and Yuan Z 2016 *npj Quantum Inf.* **2** 16025
[3] Cozzolino D, Da L B and Bacco D 2019 *Adv. Quantum Technol.* **2** 1900038
[4] Hassanpour S and Houshmand M 2016 *Quantum Inf. Process.* **15** 905
[5] Ren J G, Xu P, Yong H L, *et al.* 2017 *Nature* **549** 70
[6] Bennett C H, Bernstein E, Brassard G and Vazirani U 1997 *SIAM J. Comput.* **26** 1510
[7] Shahandeh F, Lund A P and Ralph T C 2019 *Phys. Rev. A* **99** 052303
[8] Beale S J, Wallman J J, Gutiérrez M, Brown K R and Laflamme R 2018 *Phys. Rev. Lett.* **121** 190501
[9] Chao R and Reichardt B W 2018 *Phys. Rev. Lett.* **121** 050502
[10] Roffe J 2019 *Contemp. Phys.* **60** 226
[11] Cramer J, Kalb N, Rol M A, Hensen B, Blok M S, Markham M, Twitchen D J, Hanson R and Taminiau T H 2016 *Nat. Commun.* **7** 11526
[12] Grassl M, Kong L, Wei Z, Yin Z Q and Zeng B 2018 *IEEE Trans. Inf. Theory* **64** 4674
[13] Lidar D A, Bacon D and Whaley K B 1999 *Phys. Rev. Lett.* **82** 4556
[14] Kwiat P G, Berglund A J, Altepeter J B and White A G 2000 *Science* **290** 498
[15] Chen M, Kuang S and Cong S 2017 *J. Frankl. Inst.* **354** 439
[16] Friesen M, Ghosh J, Eriksson M A and Coppersmith S N 2017 *Nat. Commun.* **8** 15923
[17] Pokharel B, Anand N, Fortman B and Lidar D A 2018 *Phys. Rev. Lett.* **121** 220502
[18] Viola L, Knill E and Lloyd S 1999 *Phys. Rev. Lett.* **82** 2417
[19] Pryadko L P and Quiroz G 2009 *Phys. Rev. A* **80** 042317
[20] Du J, Rong X, Zhao N, Wang Y, Yang J H and Liu R B 2009 *Nature* **461** 1265
[21] Almog I, Sagi Y, Gordon G, Bensky G, Kurizki G and Davidson N 2011 *J. Phys. B: At. Mol. Opt. Phys.* **44** 154006
[22] Cao W C, Liu X S, Bai H B and Long G L 2007 *Sci. China Ser. G-Phys. Mech. Astron.* **51** 29
[23] Harraz S, Cong S and Nieto J J 2022 *Int. J. Quantum Inf.* **20** 2250007
[24] Wang M J, Xia Y J, Li Y D, Yang Y, Cao L Z, Zhang Q W and Zhao J Q 2020 *Int. J. Theor. Phys.* **59** 3696
[25] Li Y L, Zu C J and Wei D M 2019 *Quantum Inf. Process.* **18** 2
[26] Branczyk A M, Mendonca P E M F, Gilchrist A, Doherty A C and Bartlett S D 2007 *Phys. Rev. A* **75** 012329
[27] Gillett G G, Dalton R B, Lanyon B P, Almeida M P, Barbieri M, Pryde G J, O'Brien J L, Resch K J, Bartlett S D and White A G 2010 *Phys. Rev. Lett.* **104** 080503
[28] Yang Y, Zhang X Y, Ma J and Yi X X 2013 *Phys. Rev. A* **87** 012333
[29] Xiao X and Feng M 2011 *Phys. Rev. A* **83** 054301
[30] Harraz S, Cong S and Kuang S 2019 *J. Syst. Sci. Complex.* **32** 1264
[31] Harraz S, Cong S and Shuang F 2018 *IEEE 7th Data Driven Control and Learning Systems Conference*, May 25–27, 2018, Enshi, China, p. 302
[32] Korotkov A N and Keane K 2010 *Phys. Rev. A* **81** 040103
[33] Kim Y S, Lee J C, Kwon O and Kim Y H 2012 *Nat. Phys.* **8** 117
[34] Wakamura H, Kawakubo R and Koike T 2017 *Phys. Rev. A* **96** 022325
[35] Wakamura H, Kawakubo R and Koike T 2017 *Phys. Rev. A* **95** 022321
[36] Wang C Q, Xu B M, Zou J, He Z, Yan Y, Li J G and Shao B 2014 *Phys. Rev. A* **89** 032303
[37] Harraz S, Cong S and Li K 2020 *Quantum Inf. Process.* **19** 250
[38] Huang J H and Zhu S Y 2007 *Phys. Rev. A* **76** 062322
[39] Knoll L T, Schmiegelow C T and Larotonda M A 2014 *Phys. Rev. A* **90** 042332
[40] Yang W, Ma W L and Liu R B 2016 *Rep. Prog. Phys.* **80** 016001
[41] Harraz S, Cong S and Nieto J J 2021 *Eur. Phys. J. Plus* **136** 851
[42] Nielsen M A and Chuang I 2002 *Am. J. Phys.* **70** 558
[43] Mendonca P E M F, Napolitano R J, Marchiolli M A, Foster C J and Liang Y C 2008 *Phys. Rev. A* **78** 052330
[44] Liang Y C, Yeh Y H, Mendonca P E M F, Teh R Y, Reid M D and Drummond P D 2019 *Rep. Prog. Phys.* **82** 076001
[45] Pirandola S, Eisert J, Weedbrook C, Furusawa A and Braunstein S L 2015 *Nat. Photon.* **9** 641